SEVENTEENTH EUROPEAN ROTORCRAFT FORUM

Paper No. 91 – 72

FLIGHT SIMULATION MODELING IN SUPPORT OF ENGINE/AIRFRAME INTEGRATION

F.K. STRAUB, J.W. HARDING, J.M. HARRISON, J.I. DORMAN

MCDONNELL DOUGLAS HELICOPTER COMPANY

MESA, ARIZONA, USA

SEPTEMBER 24 – 26, 1991

Berlin, Germany

Deutsche Gesellschaft für Luft– und Raumfahrt e.V. (DGLR)
Godesberg Allee 70, 5300 Bonn 2, Germany

FLIGHT SIMULATION MODELING IN SUPPORT OF ENGINE/AIRFRAME INTEGRATION

F.K. Straub, J.W. Harding, J.M. Harrison, J.I. Dorman
McDonnell Douglas Helicopter Company
Mesa, Arizona, USA

Abstract

The AH-64 helicopter, currently powered by two GE-T700-701 engines, is being upgraded to -701C powerplants with increased perfomance and digital engine controls. This paper presents the validation of a helicopter flight simulation model, FLYRT, for investigations of engine/airframe compatibility. First, typical engine response and controllability issues that can be encountered are discussed. Then the basis of the FLYRT model is reviewed and pertinent details of the three engine types modeled in this study are presented. The capability of FLYRT to predict engine/airframe dynamic response is validated through extensive correlation with aggressive autorotation recovery, unmask/remask, and roll reversal flight test maneuvers. Roll reversals require use of the blade element version of the rotor model in order to predict the high torque spike characteristic of this uncompensated maneuver. Having established FLYRT as a valid tool, response problems and proposed design solutions can now be readily investigated using FLYRT engine/airframe simulations.

Notation

ASA	acceleration schedule anticipator
DASE	digital automatic stabilization equipment
DEC	digital engine control
ECU	electrical control unit
FLYRT	fly real time, MDHC flight simulation code
HIGE	hover in ground effect
HMU	hydro-mechanical unit
LDS	load demand spindle
PAL	power available lever
TDI	transient droop improvement
g_{norm}	normal acceleration
Ng	gas generator speed
Np	power turbine speed
Nr, Ω_r	rotor speed
P3	compressor discharge pressure
p_B	roll rate
Qr	rotor torque
Qt	engine torque
T45	turbine inlet temperature
Wf	fuel flow
δ_0, δ_c	colective and lateral cyclic controls
ϕ	roll angle

Introduction

The McDonnell Douglas Helicopter Company (MDHC) AH-64A Apache helicopter is powered by two General Electric (GE) T700-GE-701 engines. As part of continuing improvements to enhance the aircraft's capability, uprated T700-GE-701C powerplants have been installed. These new powerplants have increased power, providing the AH-64A with improved high altitude capability. In addition, part of the engine control system has been converted from analog (ECU) to digital (DEC) operation, providing increased reliability, lower cost, and ability to tune the controls.

Engine/airframe integration plays an important role in handling qualities, in particular for highly maneuverable and agile helicopters such as the AH-64A. Engine response and controllability must be tuned to properly deal with the rotor dynamics during aggressive maneuvers. Since stand-alone engine tests are typically only conducted in steady conditions with the objective of providing flight performance type data, computer simulations must be relied upon to optimize the engine control system and evaluate the engine/airframe response behavior before flight testing.

MDHC's FLYRT (Fly Real Time) flight simulation model, references 1 and 2, represents a detailed model of the AH-64A helicopter. It includes models of the main rotor, fuselage, horizontal stabilator, vertical

stabilizer, tail rotor, landing gear, engine, engine control, drive train, and flight control system. The main rotor is modeled using a quasistatic table lookup approach, enhanced with closed form solutions for transient effects. This table, also called rotormap, contains six rotor states as function of collective pitch, advance ratio and inflow, and is generated off-line. Alternately, the main rotor is modeled using a blade element model, providing a more rigorous treatment of transient effects. The engine and engine control models are based on information provided by GE (see also ref.3). The FLYRT rotormap model has been well validated for basic flight dynamic and maneuver analysis, references 4 and 5.

The 701C powerplant has a maximum continuous rating of 1682 HP (418 ft-lb torque) at SLSTD conditions, compared with 1510 HP (379 ft-lb) for the 701. An interim version of the DEC equipped 701C, hereafter called Mod2, was flight tested in the AH-64 during early 1990. During aggressive autorotation recoveries, decel/accel, and roll reversal maneuvers several response and controllability issues were encountered. As a result, design modifications were made, leading to the 701C Mod3 configuration, which was prepared for integration and flight tested during the present study.

The basic objective of the work reported here is to validate FLYRT as a simulation tool to assess engine and engine control designs, guide and evaluate parametric design studies, and demonstrate engine/airframe dynamic compatibility before flight testing. The detailed objectives of this study are:

1. Validate the dual engine model version of the Apache FLYRT, with 701 engines. Establish FLYRT as tool to address 701C engine/airframe integration issues.

2. Incorporate the 701C Mod2 engine and fuel control model into FLYRT and validate with flight test data gathered during the first half of 1990.

3. Incorporate the latest engine modifications, 701C Mod3, into FLYRT and verify its operation. Conduct simulations to evaluate engine/airframe integration, and validate with flight test data as it becomes available.

The paper presents a detailed description of the simulation effort. First, typical engine response and controllability issues are discussed. A brief description of the Apache FLYRT simulation model, the structure of the engine model, and some specifics of the 701, 701C Mod2, and 701C Mod3 engines are provided. Analytical studies conducted to evaluate engine/airframe compatibility are briefly summarized. Results for a roll reversal maneuver illustrate the reasons why the blade element model must be used for adequate fidelity. The approach taken for validation and results, comparing FLYRT predictions with flight test data, are presented. FLYRT predictions for roll reversals are made with both the rotormap and the blade element main rotor models and are compared with each other. Finally conclusions from this study are presented.

Engine Integration Challenges

When integrating a new engine with an airframe, several engine response and controllability problems can occur during aggressive maneuvers. Particularly problematic are autorotation recovery, unmask/remask, and decel/accel maneuvers, all with substantial collective inputs. Of the uncompensated maneuvers, i.e. those without collective input, roll reversals are most critical. Problems encountered can be torque overshoot, torque rollback, torque mismatch and torque swapping, and rotor droop. Figure 1 illustrates these characteristics in a severe 1.2 sec and a moderate 5 sec collective pull during autorotation recovery.

Transient Torque Overshoot. Temporary overshooting of required torque, relative to the final steady state value, can occur following rapid collective control increases. Overtorquing hinders a pilot's ability to control the aircraft. The major concern is exceedance of transmission and drive train torque limits, in particular at cold and low altitude conditions where more engine torque is available. Overtorquing is an inherent problem in engines with turbine speed (Np) governing.

Rotor Droop. Rotor droop results from either the engine power section not being capable of supplying the torque required to meet the aircraft's demand, or the fuel flow control not being satisfactory in anticipating and responding to aircraft torque needs. Torque demand is largely driven by rotor inertia, thus requiring engine optimization to accommodate aircraft with different rotor inertias. Excessive droop mostly occurs during autorotation recoveries. Initially the rotor is at overspeed condition and the engine is at zero power (flight idle). Collective application causes the rotor speed to decay. Load anticipation circuitry stimulates Np to rise above its 100% nominal isochronous (Np governor reference) value

and meet Nr on its decay downward. The clutch is disengaged up until Nr equals Np. Rotor speed then decreases further, at the expense of stored kinetic energy, until power available equals power required.

Rollback. Rollback is seen, in certain maneuvers with moderate collective application, as a short term decline in fuel flow and engine torque output, while collective is still being increased. As a result the pilot experiences insecurity. Rollback is mostly driven by interaction and switching of engine control laws, rather than by airframe torque demands.

Torque Swapping. Torque swapping can appear in twin engine configurations. It manifests itself as one of the two engines showing a higher torque output, followed in time by showing a lower torque compared to the other engine. This may be repeated in several cycles. The cause of torque swapping, or the two engines in an aircraft not behaving identically, may lie in both differences in the engine themselves, or the interface with the aircraft, such as control linkages and spacial mounting differences. Continual changes in engine performance and efficiency cause engine differences to be time-varying. Feedback is used to minimize engine torque output differences by raising the output of the low engine. The torque matching (torque sharing) logic in each engine acts if the torque of an engine is low by 2% or more compared to that of its mated engine; however, the torque matching commands are also limited by the accel schedule.

FLYRT

The AH-64 engineering simulation code, referred to as FLYRT, was developed by MDHC over the past decade (ref. 1 and 2). It is used extensively in a manned simulation mode for investigation of helicopter flying qualities. In the batch mode, it is used for studying handling qualities and flight control law development during the design phase. FLYRT has been validated against flight test data using both open loop step control inputs and emulating specific maneuvers (ref. 4 and 5).

Overview

In FLYRT, the main rotor consists of a hybrid model which is a combination of a quasi-static rotormap and a closed form analytical solution to account for transient effects. The rotormap is generated off-line by a nonlinear blade element model with a flap degree-of-freedom and consists of a table of six rotor states (coefficients of rotor disk loading, shaft torque, in-plane forces, and longitudinal and lateral cyclic flapping angles) as a function of three performance parameters in the control plane of reference (collective pitch at 3/4 radius, advance ratio, and inflow ratio). The rotormap generation and its utilization within FLYRT is a unique procedure which is computationally efficient, making it amenable to real time application. An option does exist, in the batch environment, for replacing the rotormap with the full nonlinear blade element model used to create it. This approach provides a more rigorous treatment of transient effects which play an important role in the uncompensated roll reversal maneuvers discussed later.

The anti-torque system comprises the tail rotor and vertical stabilizer. Because of their close proximity, there is a strong mutual aerodynamic interference which is modeled in an iterative loop. The vertical surface aerodynamic characteristics are data dependent. Three-dimensional lift and drag coefficients are computed as functions of angle-of-attack. The tail rotor is modeled in linear closed analytical form using strip/momentum theory. The aerodynamic characteristics of the horizontal stabilator are treated in a fashion similar to the vertical stabilizer. Its incidence is variable, driven by a schedule based on indicated airspeed, main rotor collective, and body pitch rate. The fuselage/wing combination is modeled as a single unit including engine nacelles (unvented) and all appendages pertaining to the Apache operational role.

The six rigid body degrees-of-freedom of the helicopter are dynamically coupled to the main rotor. The drive train is represented as a two degree-of-freedom flexible model with dynamic coupling between main rotor as one branch, engines and anti-torque system as the other branch. The system is dynamically coupled to the body roll and yaw through the main rotor. The engine is modeled in sufficient detail to cover performance from flight idle through all phases of flight, including ground modes such as take-off, landing, and taxi. The landing gear is modeled as three independent units interfacing with a rigid airframe. The flight control system model is detailed sufficiently for handling qualities and stability studies. It includes a model of the digital automatic stabilization equipment (DASE). In the time integration module, Euler angles are computed by quaternions to avoid singularities during large attitude maneuver simulations. In the batch mode, FLYRT has provision for a "paper" pilot model which combines application of prescribed flight control inputs with

an adaptive control system to perform specific maneuvers. In addition, a linear perturbation model with eight states can be generated about any trimmed state.

Engine Models

All AH-64 FLYRT simulation models used in this study feature dual engine models adapted from the original data base, computer code, and relevant flow diagrams provided by the manufacturer. The models represent, in detail, the current T700-GE-701, the 701C Mod2 and the 701C Mod3 versions as defined by GE. The differences between the 701 and 701C models are in the engine performance data and the modeling of the engine control (which is analog (ECU) for the 701, versus digital (DEC) for the 701C version). The basic structure of the FLYRT engine model, as discussed below for the 701, is preserved throughout.

The engine model is built around the gas generator unit which is described dynamically as a single degree-of-freedom subsystem. Instantaneous speed and discharge pressure determine the performance of the other units. The power turbine is treated dynamically as an integral part of the drive train, so that the only significant output is engine torque. The gas generator is controlled by the hydromechanical unit (HMU) which feeds fuel as a function of load demand spindle (LDS) position, power available lever (PAL) position and the demanded output of the ECU or DEC. This fuel flow is further subjected to limitations of acceleration, deceleration and idle schedules, in order to protect the engine from compresser stall or flameout. Thus fuel is metered as a function of compressor discharge pressure (P3), commands from the the electrical control unit (ECU/DEC), and the pilot's control. The pilot command inputs are imposed through the PAL, mounted in the cockpit, and the LDS, which is linked mechanically to the collective pitch lever. Input from the collective pitch generates a load anticipation command. The PAL has only two positions in normal use, "idle" and "fly", however, it can also be used in a proportional sense when in "lockout" mode, (there the PAL is used as a hand throttle with the ECU/DEC inactive). The ECU/DEC serves to control the entire engine system subject to pilot inputs. Its main function is to process the power turbine speed error through a position-rate-integral law designed to maintain that speed within close limits – "isochronous" control. In this function, it is aided by supplementary load anticipation algorithms based on collective pitch rate, torque and power turbine output speed signals. The ECU/DEC imposes restraints on fuel flow as a function of power turbine inlet temperature (T45) and attempts to minimize any torque differential between the power turbines of the two engines, by increasing the reference speed (and thus fuel flow) of the low torque engine.

Each engine has been modeled as two major components, the engine and the integrated control system. The engine is subdivided further into five thermodynamic entities. These are the air intake, the gas generator, the power turbine, and two heat sinks. The first three are readily identifiable as described above. The heat sinks are conceptual and form part of the turbine system. The control system has three subsections; the HMU which carries out fuel metering operations, the ECU/DEC, and the mechanical inputs from the pilot.

The basic goal in designing the 701C Mod3 engine controls, as compared to the 701C Mod2, was to reduce transient torque overshoot during aggressive maneuvers, while maintaining minimal Nr droop. To accomplish this, two major features were introduced by GE in the Mod3: 1) an accel schedule anticipator (ASA), which limits Ng governor overtravel during rapid load application; this acts to smooth the engine response following an accel schedule limiting event; 2) modifications to the governor to take advantage of the ASA. In addition, minor changes were made to to the accel schedule (slightly increased at the upper end) and the torque sharing time constant (which was reduced in order to improve torque matching).

Analytical Studies

The analytical maneuvers simulated during the study are intended to explore a full range of critical flight conditions that push the engine/airframe dynamic interface to its limits. This allows a rational assessment of the effectiveness of engine and engine control system designs, and highlight any problem areas. Results from such simulations can potentially be used to make a go/no-go decision for flight testing or alert the pilot to problem areas. In addition, analytical studies are perfomed to: evaluate configurations and conditions that are not readily flight tested; investigate problems experienced during flight test; and conduct parametric studies to guide future design updates.

First, a set of referee maneuvers, which are included in the engine/airframe interface requirements agreement, were simulated. They include autorotation re-

covery, unmask/remask, and roll reversal maneuvers similar to those selected for the validation studies presented above. Additional maneuvers are quick stop, decel accel, terrain approach, and ridgeline crossing. Next, autorotations at alternate altitudes that could not be flown were investigated. They are sea level at high gross weight, 10000ft, and 1000ft at 0deg F. The effect of dissimilar engines, with deviations in the accel schedule and the steady-state operating line that are representative of manufacturing tolerances, was investigated for autorotation and decel/accel maneuvers. Alltogether, about 100 simulation runs were made. No results are presented since this part of the study is on-going. However, a brief discussion of the execution of analytical maneuvers in FLYRT and a description of the critical maneuvers follows.

Execution of Analytical Maneuvers

Flying of maneuvers in the FLYRT batch mode is accomplished using the "paper" pilot model, which combines application of prescribed flight control inputs with an adaptive control system to perform specified maneuvers. Maneuvers are normally executed with DASE 'on' in all three axes. The "paper" pilot has three features:

1. Prescribed input profiles, formally programmed for any of the four control axes.
2. A 3-axis constraint pilot mechanized as a variable gain, full authority, stability augmentation system.
3. A multi-law, 4-channel adaptive auto-pilot.

Maneuvers are carried out serially in discrete stages. Passage from stage to stage is effected at specified times or when pre-determined criteria are satisfied, each criterion being a function of aircraft state trajectory. The criteria thus constitute decision points based on pilot judgement. Each stage is associated with its own package of control inputs which may or may not be varied during progress through the stage. The stages are discrete only in that the control laws change from stage to stage. Physically there is no discontinuity, and some laws could be active throughout an entire maneuver.

Prescribed inputs, item 1 above, are imposed incrementally at each time frame. They follow a simple law with constant increments subject to upper and lower limits and can be active in any of the four control channels (pitch, roll, yaw, and vertical). These raw commands are supplemented by the adaptive control laws, item 3 above. They serve to fine tune the response, smoothing what would otherwise be a bang bang system. The constraint pilot, item 2 above, serves as a passive agent, a means of suppressing unwanted response about "off" axes.

Maneuver Description

The quick stop maneuver is a deceleration from a predetermined steady-state condition (120 kts) in level flight to a hover state, holding height constant within tolerance.

The decel/accel maneuver is a deceleration from a predetermined steady-state condition (120 kts) to an interim speed (60 kts), followed by an acceleration to the initial speed or V_h.

The terrain approach maneuver is executed as a transition from a predetermined steady state condition (120 kts), within a specified height band above local terrain, terminating in a hover within ground effect. Loss of height is achieved in a descending turn with a finite needle split (Nr/Np) not less than a specified magnitude. This maneuver is closely related to the quick stop.

The roll reversal maneuver objective is to roll right (left), to a 60 degrees bank angle applying lateral stick at a rate of 100% full travel per second. With some anticipation, so that required attitude is not exceeded, the stick is reversed to attain a 60 degrees bank angle left (right), again with application at 100% full travel per second. The stick is then centered to return to a "wings" level state. Some activity is required in the longitudinal axis to control pitch attitude. There is no activity in the other two axes, and the aircraft is allowed to yaw freely as if in a coordinated turn.

The autorotation recovery is not so much a maneuver as a programmed procedure, with the objective to demonstrate recovery from autorotation in a specified steady-state flight configuration (80 kts). Three variables are considered: 1) the starting state Nr/Np split; 2) the rate at which collective pitch is applied during recovery; 3) the end state power level. Two approaches, namely flying into autorotation and trimming in autorotation, are used. The latter approach is preferred, since it provides repeatability and reduced computational times.

The unmask/remask maneuver requirements are to initiate the task from HIGE, pull collective to 100% torque at 100 %/sec control rate. Collective is held at that position for 2 seconds then dropped 3.8 degrees

at 50 %/sec. After 3 seconds, collective is pulled to the original trim value at 50 %/sec.

The ridgeline crossing maneuver is initiated at 120 knots. From 120 knots, collective is dropped 5 degrees at 25 %/sec and held down for 3 seconds. Collective is then pulled 7 degrees at 25 %/sec and held to complete the maneuver.

Results

Roll Reversal Using Blade Element Model

Typical time histories for a right roll reversal maneuver at 120 kts are shown in figure 2, showing a) lateral cyclic input and blade flapwise displacement, b) roll rate, c) power turbine speed, and d) the torques generated in the main drive train components. This uncompensated maneuver is marked with a torque spike in the main rotor drive shaft influenced by the high rate of left roll during the reversal. The engine responding, generates a matching spike. As shown in figure 2d, the two spikes are approximately in phase. In order to simulate these phenomena with any pretensions to fidelity, it is necessary to employ the blade element version of the main rotor model in FLYRT.

Blade response for two rotor revolutions during the approach to maximum right bank angle (first time slot, 2.0 to 2.4 sec in fig. 2) is shown in figure 3. Blade element quantities are shown at station 0.85R. Blade flapping is characterized by a large positive (upward) velocity in the downwind sector (fig. 3a), which is reflected in the helix angle (φ_H = negative inflow angle) profile (fig. 3b). The lift and drag profiles are substall (fig. 3c). Thus, lift contributions dominate and, because of the large negative helix angles, lead to the blade (aerodynamic) torque peak in the fourth quadrant (fig. 3c). This peak increases from one revolution to the next, leading to the first main rotor torque peak in figure 2d.

Blade response for two rotor revolutions during the time period spanning the roll reversal from right to left (second time slot, 3.2 to 3.6 sec in figure 2) is shown in figure 4. Compared to the first time slot, the flapping displacement has peaked and reversed (fig. 2a) under the left roll response. Figure 4a shows the flapping velocity profile reversed in sense, which is reflected in the helix angle profile in figure 4b. The influence of a negative flapping velocity in the downwind sector is dominant, leading to large angles of attack (α) and driving the blade element into deep stall as shown in figure 4b. The stall induces a large drag peak (fig. 4c) which in turn dominates the blade torque profile although there is some tempering by the lift component, which contributes an accelerating torque component by virtue of the reversed (positive) helix angle profile. The end result of this sequence is that there are two main rotor torque peaks spaced about one second apart, the first being the larger. They are preceded by a deep trough and separated by a shallow one. The first trough and peak are more important.

Engine governing during this type of maneuver with no compensating collective inputs relies solely on engine speed sensing and control. The sudden decrease in main rotor torque during maneuver entry, see figure 2d, results in a rotor/engine overspeed excursion as shown in figure 2c. In turn the engine controls are activated to decrease engine output which reaches minimum as the first main rotor torque peak occurs. A significant underspeed occurs, and correction of this underspeed leads directly to the engine torque spike. The second main rotor torque peak contributes to the intensity of the spike by prolonging the underspeed excursion as is apparent from figure 2c. The main rotor drive shaft, oscillating at the drive train first modal frequency complicates the issue as do the engine control characteristics. Nevertheless, the primary mechanism is located in the main rotor and is inherent in the dynamic and aerodynamic characteristics. Response to the control input and subsequent airframe motion is influenced only by the variation in angular velocity. Amelioration of the engine torque response could be achieved by softening the governor or limiting output torque.

The reason for using the blade element model is clear from the above analysis. The main rotor torque is compounded from the contributions of the individual blades each of which responds differently from the others by virtue of relative phasing. The phenomena cannot be reproduced accurately by the rotormap model. The rotormap itself is quasi-static and generated using a single representative blade. The transient components of the main rotor states are computed using a linear closed form analytical model and do not reflect changes in lift or drag due to local stall or Mach number effects.

Correlation

To validate FLYRT as a tool for engine/airframe integration, several flight test cases are selected that exhibit significant dynamic interaction between the engine/rotor/drive train system. Maneuvers consid-

ered are autorotation recovery, unmask/remask, and roll reversals. The fast collective pull exercises the acceleration schedule in isolation from the Np governor. A slow autorotation recovery with an 8 second pull isolates the Np governor with no HMU schedule limiting. The unmask/remask shows a sharp collective pull from a high torque condition resulting in a torque overshoot above 100 percent. The remask portion of the maneuver has a collective drop sufficient to put the engines on the deceleration schedule, again in isolation from the Np governor. Roll reversals are included to show the engine response to uncompensated maneuvers. Both left and right roll reversals show a characteristic torque rise during high left roll rate conditions.

Approach. Calculated responses are obtained by trimming the model to the appropriate flight condition and then driving the simulation model with measured control time histories. Pressure altitude, temperature, gross weight, and c.g. position are set to flight test values. For autorotation maneuvers, trimming into autorotation involves matching the main rotor overspeed. The gross weight is reduced from the take-off value to reflect fuel burned inflight prior to performing the particular maneuver.

The model is flown DASE-on with the longitudinal, lateral, directional, and collective controls driven by the measured pilot control signals. This process involves converting the measured controls to perturbation controls by subtracting the initial values. The model is driven by adding the perturbation controls to the trimmed model control positions to simulate exact pilot control motion in four axes. With this method, initial condition errors in controls do not effect the dynamic response. In addition to the four primary controls, measured load demand spindle (LDS) angles are used to drive the engine by disabling the LDS angle calculations in the model. Engine response is sensitive to LDS changes which are subject to the dynamics of the mechanical link between the collective actuator and the LDS. Using the measured LDS angles eliminates the effects of modeling this mechanical link and provides a better comparison of engine response.

Validation Results. Five flight test maneuvers are chosen for correlation with the FLYRT 701 and 701C models. The maneuvers include three autorotation recoveries, an unmask/remask, and two roll reversals, see table 2.

Table 1: Correlation cases

Fig.	Description
5	Autorotation recovery: 4% split, 1sec pull
6	Autorotation recovery: 8% split, 8sec pull
7	Autorotation recovery: 5% split, 7sec pull
8	Unmask/Remask: 2sec pull;
9	Lat Reversal Right: 130kts, 90deg;
10	Lat Reversal Left: 130kts, 90deg;

Figure 5 shows correlation with the fast collective pull from autorotation. It shows a characteristic engine torque rise to 100 percent (379 ft-lb) followed by a drop in torque to a steady-state value of about 78 percent. The model is driven with the measured controls and measured LDS angles from the left and right engines. Following the initial collective input, the model gets on the acceleration schedule and stays there for 4 seconds. Torque from engine 1 matches flight test while the flight test torque from engine 2 rises earlier than the model. This trend is also evident in both the pressure and gas generator speed comparisons (not shown). Both power turbines droop below the minimum flight test value of 90 percent. This excess droop could be related to the drive train model as seen in the initial main rotor torque and engine torques. Early oscillations in main rotor torque do not appear in the model resulting in a higher steady load on the engines. The engine torque drop at 5 seconds is accurately predicted and corresponds to the engines coming off the acceleration schedule. It should be noted here that rotor droop prediction is improved for the 701C models (not shown).

Correlation with the slow pull from autorotation in figure 6 shows a good match between the model and flight test. This maneuver verifies the accuracy of the Np governor model. Torque rises for the model engine 2 at 6.5 and 8 seconds are caused by the torque sharing logic trying to bring the number 2 engine up to match the number 1 engine. Correlation with an moderate pull of 7sec in figure 7 shows a reasonable match in predicting rollbacks, both at the outset (2 sec) and in the middle of the pull (6 sec). Data for this last maneuver is from 701C Mod2 flight testing, with results for the 701C Mod3 shown for comparison purposes.

The unmask/remask maneuver also shows good correlation as seen in figure 8. The gross weight for this particular maneuver was reduced (by 1000 lbs) from take-off gross weight to match engine torque.

Figures 9 and 10 show lateral roll reversals right and

left, respectively. Results are presented for both the rotormap and the blade element model. Airframe response is predicted quite well using either model. However, the rotormap model does not capture at all the changes in engine torque (Qt) that occur during the roll. The blade element model predicts both the torque rise during left roll and the torque drop during right roll qualitatively in good agreement with test data. Magnitudes of the torque rise are low, however, it should be pointed out that better results have been obtained with a later improved model (ref. 6). These results clearly illustrate the need, as discussed above, to use the blade element model in order to capture the torque spikes during left roll.

Conclusions

The present study addresses flight simulation modeling in support of engine/airframe integration for the AH-64 helicopter. The flight simulation code FLYRT is used to investigate a series of aggressive maneuvers that push the engine/airframe dynamic interface. The most critical maneuvers are autorotation recovery, decel/accel, and roll reversals since they can exhibit significant amounts of transient overtorque, droop, rollback, and torque swapping. Specific conclusions are:

1. FLYRT predictions are extensively correlated for autorotation, unmask/remask, and roll reversal maneuvers. FLYRT predicts engine and airframe response well. Droop is somewhat overpredicted and torque overshoot and rollback are underpredicted.

2. FLYRT's highly efficient rotormap approach is accurate enough for most maneuvers. To capture the dynamics of roll reversals, the blade element option must be used. It is able to predict the torque spike during left roll qualitatively correctly, however it is low in magnitude.

3. Simulation of a large set of referee maneuvers with both the 701C Mod2 and Mod3 models is accomplished in a very short time, using a combination of the efficient rotormap and the high fidelity blade element model for the compensated and uncompensated maneuvers, respectively.

4. FLYRT is readily applied to demonstrate engine/airframe compatibility in flight conditions (gross weight, altitude, temperature) and configurations (dissimilar engines) that cannot be readily tested.

In summary, FLYRT has been established as a valuable tool to investigate and validate future engine development work and demonstrate engine/airframe compatibility. It is planned to use FLYRT as a matter of course in supporting engine integration work.

Acknowledgements

This study was sponsored by the U.S. Army under contract DAAJ09-90-G-0022. The help of GE personnel in improving the engine models and integrating them into FLYRT is greatfully acknowledged. The dedicated support of MDHC staff members D.G. Ruttledge, who integrated the 701C models into FLYRT and guided the analytical studies, and J. Sorensen, who reduced parts of the flight test data, proved invaluable.

References

1. Harrison, J.M., and Shanthakumaran, P.: AH-64 Apache Engineering Simulation Engineering Manual, **USAAVSCOM TR** 90-A-011, Oct. 1990.

2. Shanthakumaran, P. et al.: AH-64 Apache Engineering Simulation Program Documentation, **USAAVSCOM TR** 90-A-012, Oct. 1990.

3. Curran, J.J.: T700 Fuel and Control System, a Modern System Today for Tomorrow's Helicopters, **Proc. 29th AHS Forum**, May 1973.

4. Shanthakumaran, P., Harding, J., and Bass, S.: AH-64 Apache Engineering Simulation Non-Real Time Validation Manual, **USAAVSCOM TR** 90-A-010, Oct. 1990.

5. Harding, J.W., and Bass, S.M.: Validation of Flight Simulation Model of the AH-64 Apache Attack Helicopter Against Flight Test Data, **Proc. 46th AHS Forum**, May 1990.

6. Harrison, J.M., and Kumar, S.: A Helicopter Flight Model Suitable for Aggressive Maneuvers, **MDHC RTTN** 91-004, March 1991.

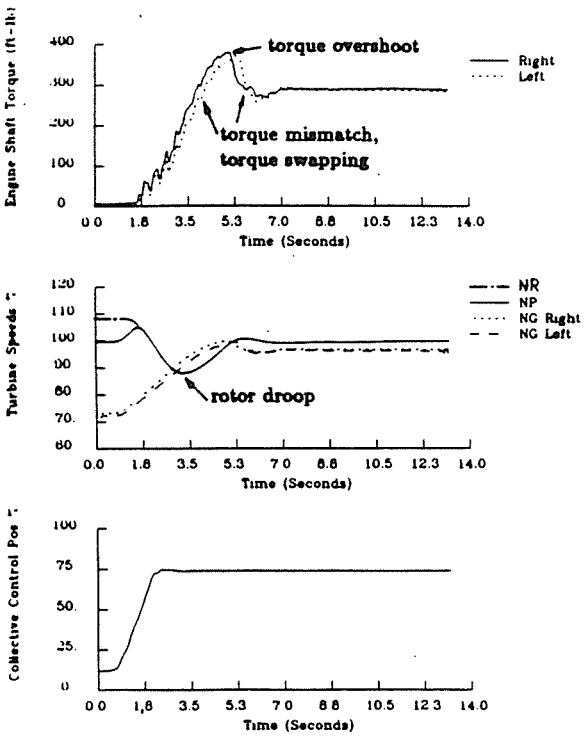

a) Fast collective pull from autorotation

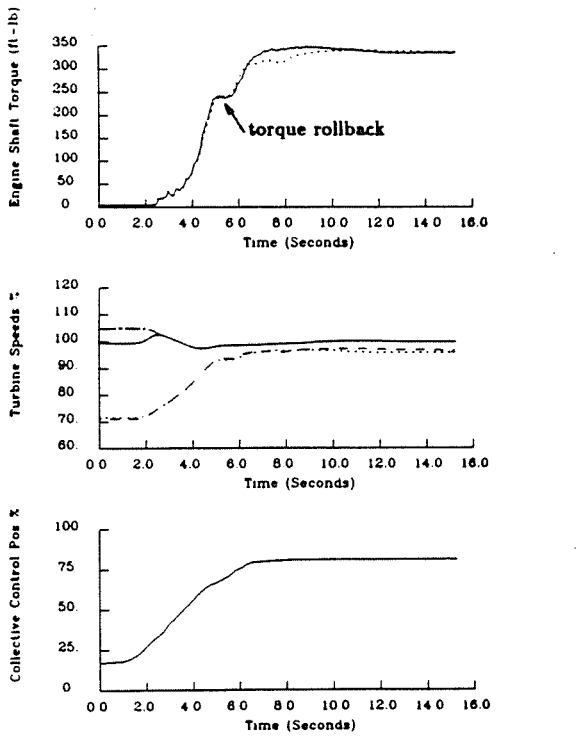

b) Moderate collective pull from autorotation

Figure 1: Engine response and controllability issues

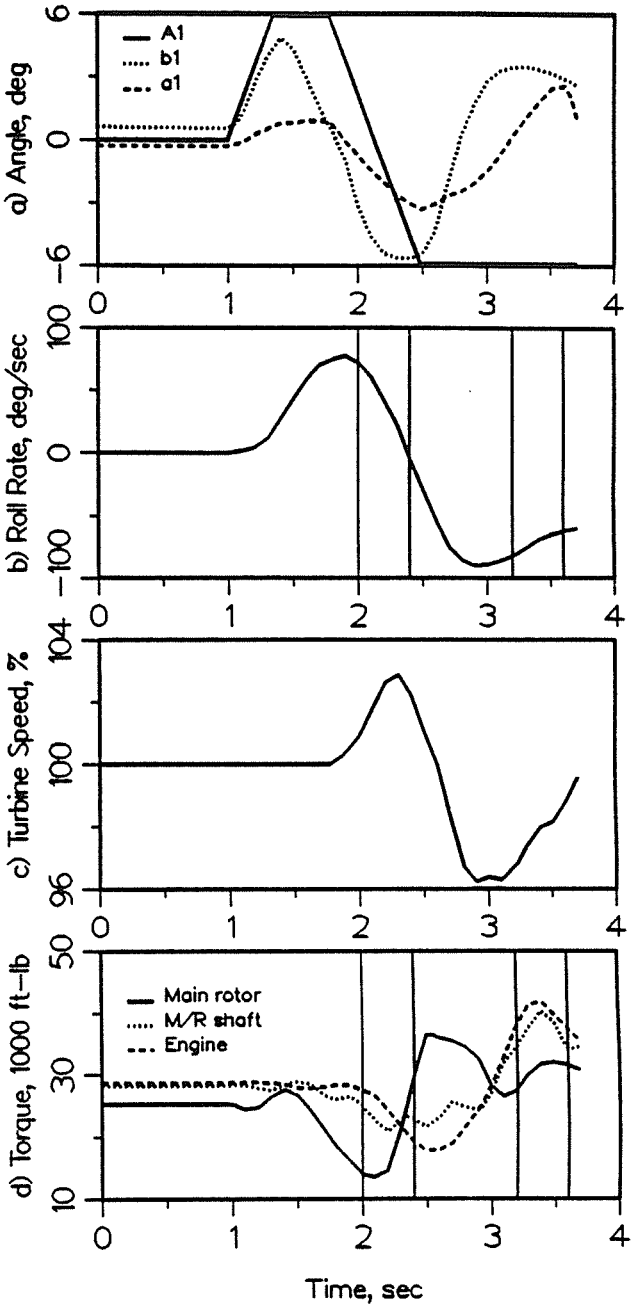

Figure 2: Right roll reversal control input and response

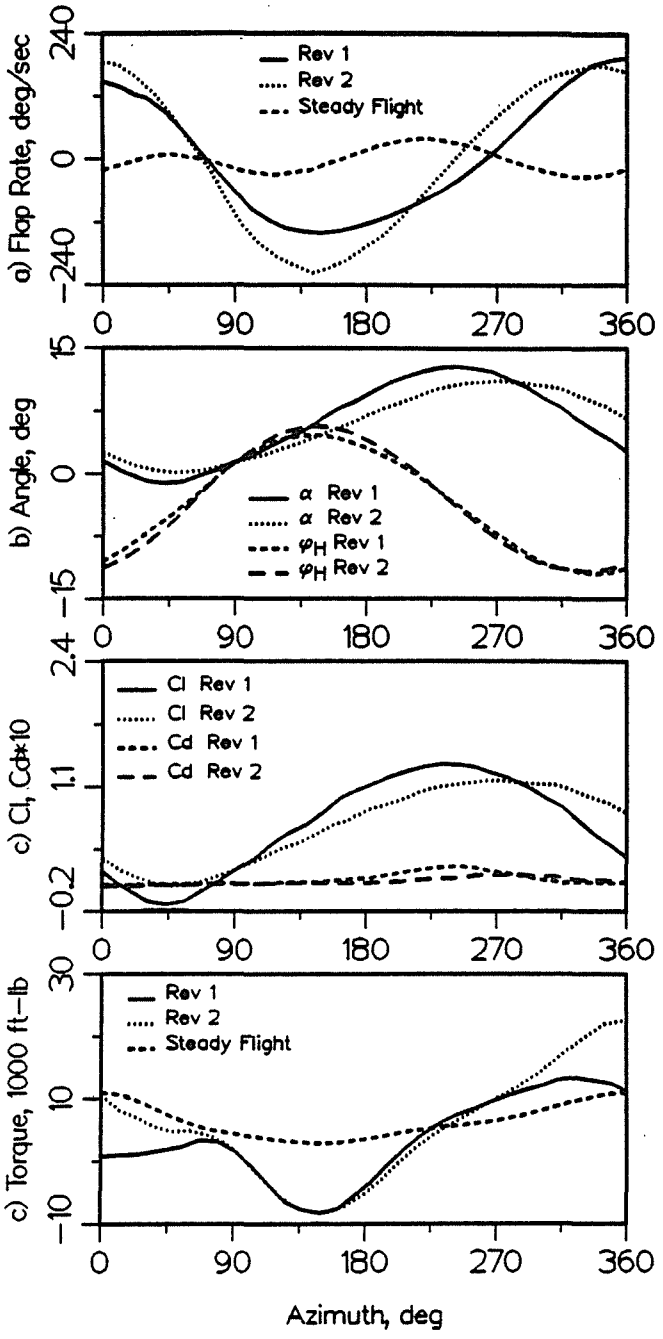

Figure 3: Blade response during approach to max right bank angle

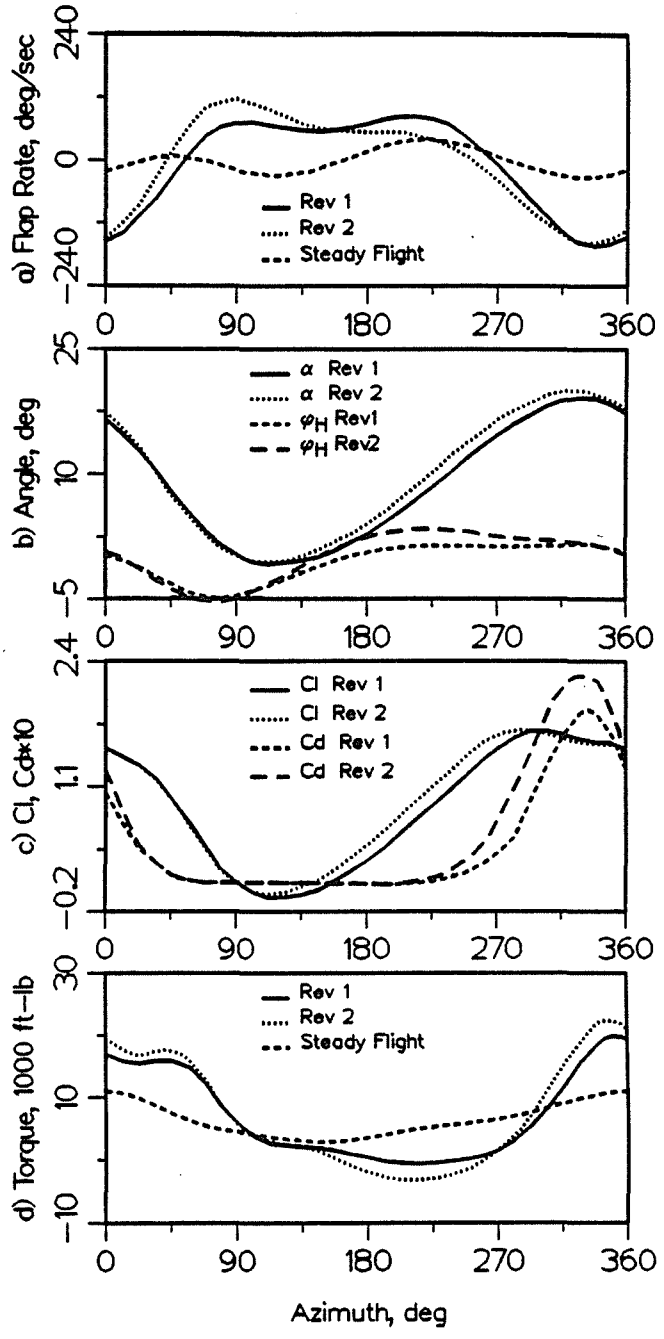

Figure 4: Blade response during reversal from right to left

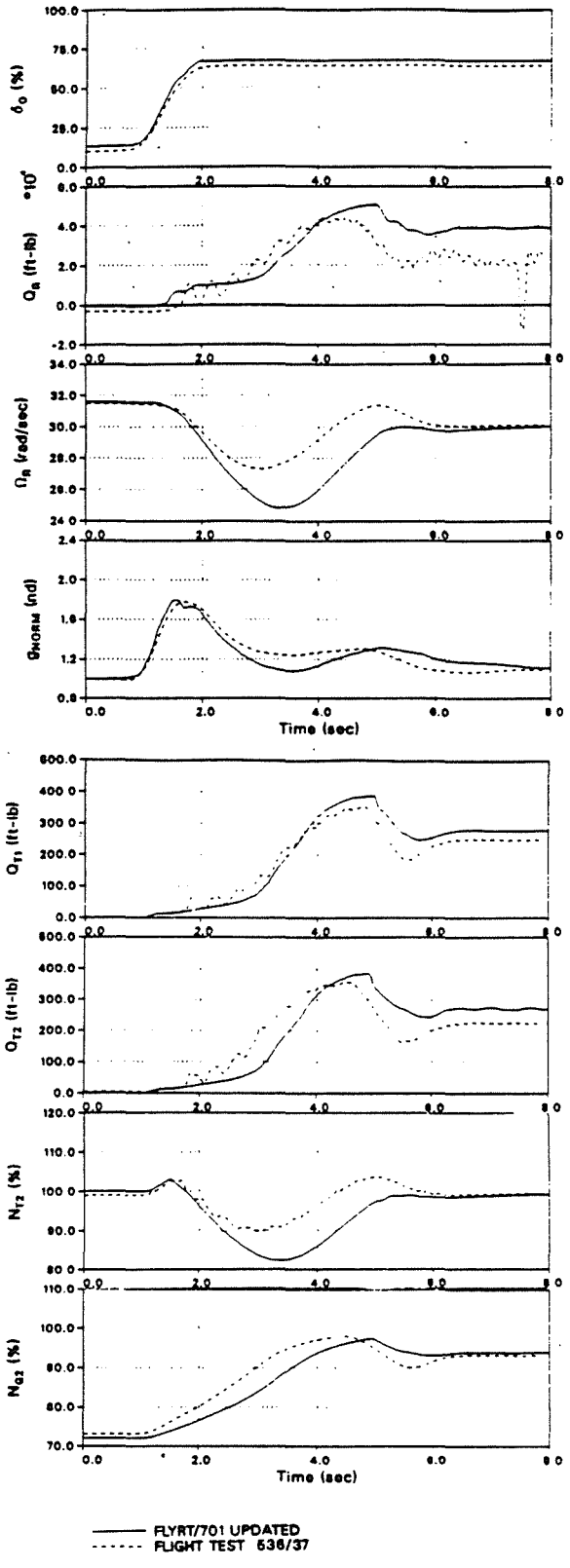

Figure 5: Fast collective pull from autorotation

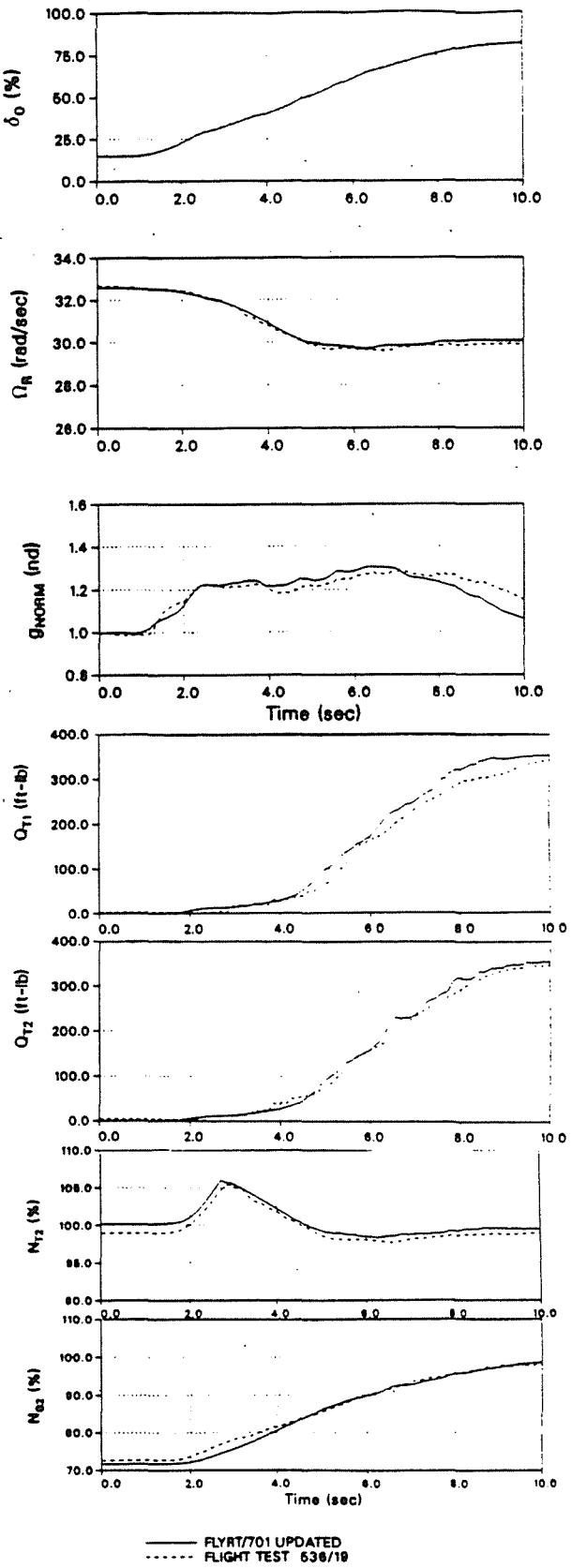

Figure 6: Slow collective pull from autorotation

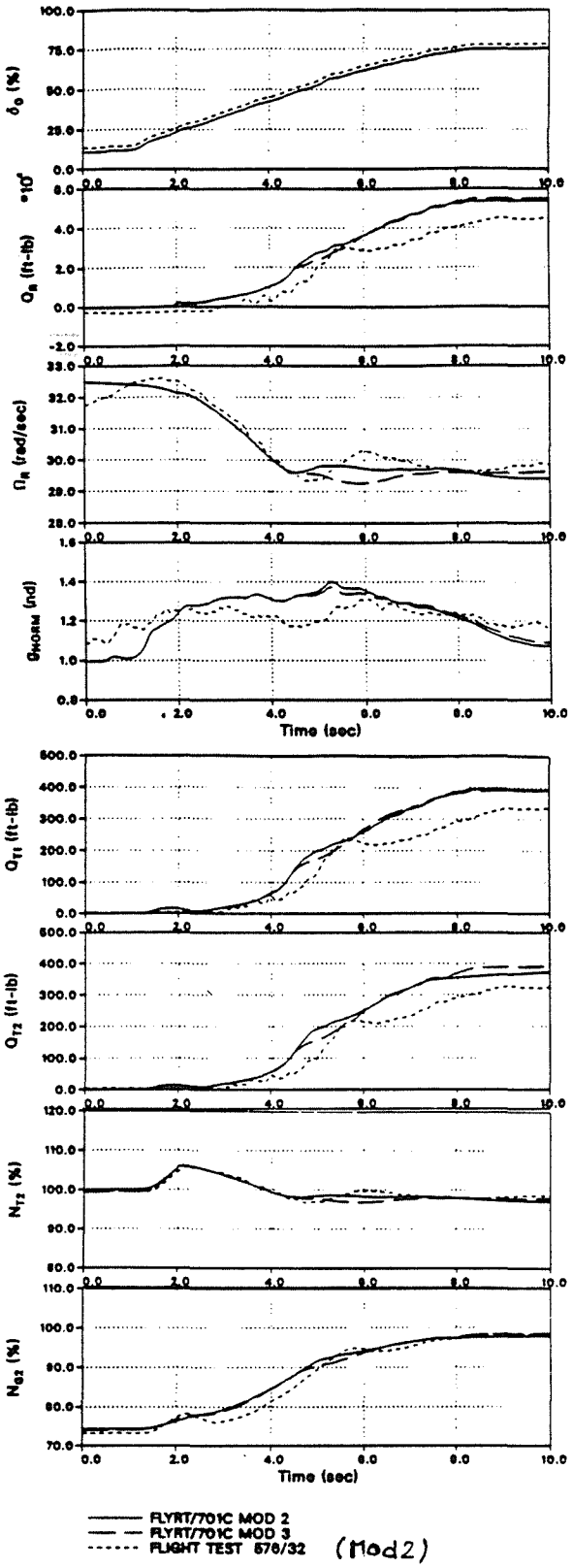

Figure 7: Moderate collective pull from autorotation

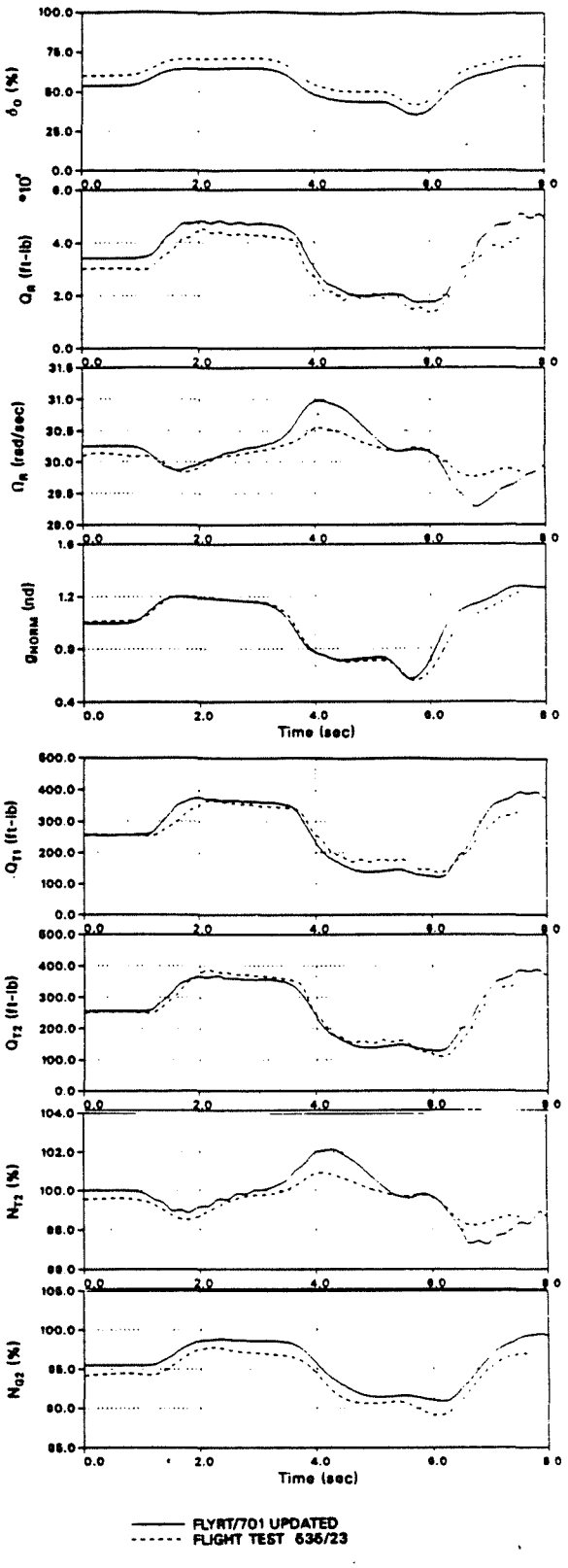

Figure 8: Unmask/remask maneuver

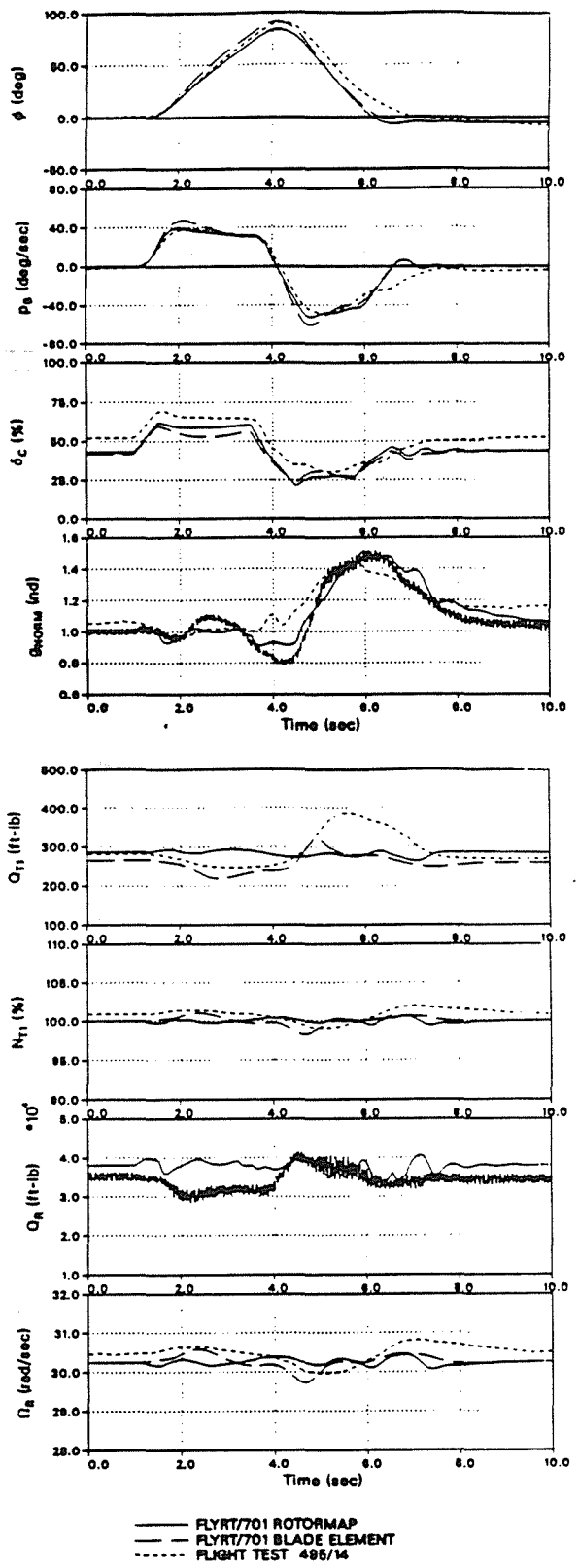

Figure 9: Right roll reversal

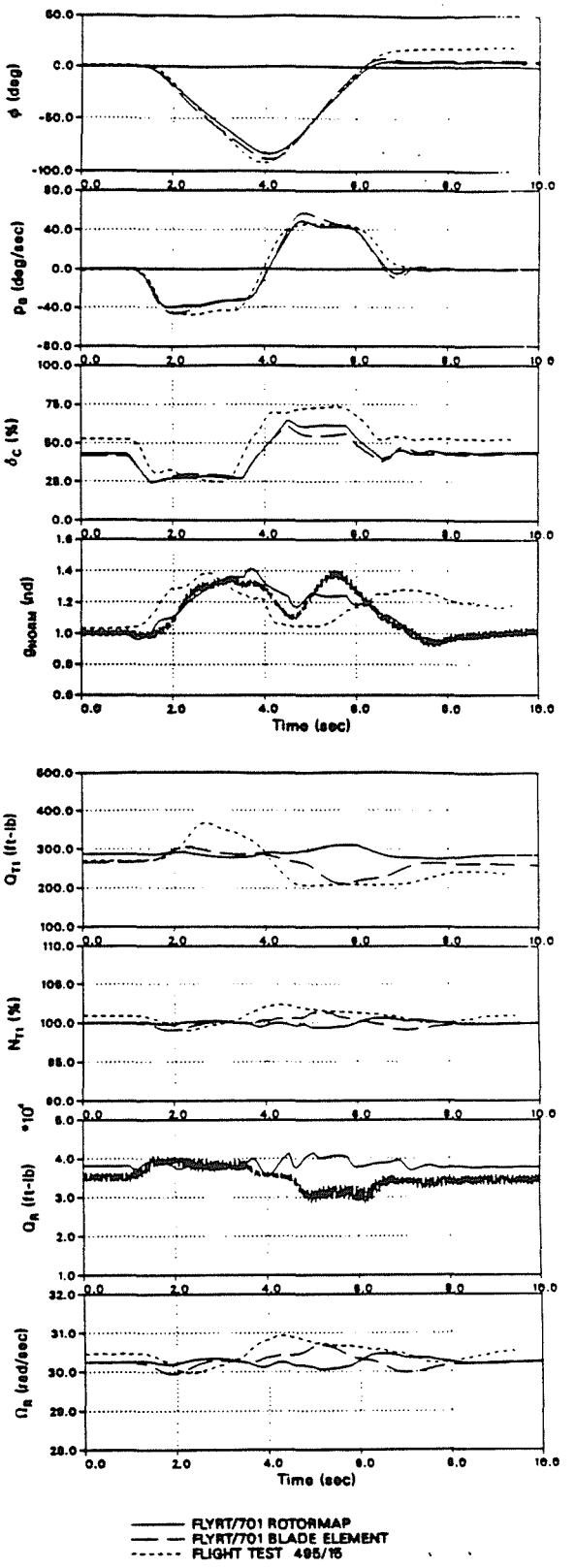

Figure 10: Left roll reversal